Supplementary Information (SI) for Nanoscale.

Supporting Information for

Universal scaling laws on rotational energy landscape for twisted van der Waals bilayers

Zichong Zhang[1], Shuze Zhu*[1]

[1]Center for X-Mechanics, Department of Engineering Mechanics, Zhejiang University, Hangzhou 310000, China

*To whom correspondence should be addressed. E-mail: shuzezhu@zju.edu.cn

1. Details for Atomistic Simulations

We begin with the notation for stacking type of various materials. For twisted bilayer graphene, AA stacking possesses the highest energy (Figure S1(a)), and AB stacking possesses the lowest energy (Figure S1(b)). The interlayer distance is greatest in AA stacking, whereas it is minimized in AB stacking [1-3].

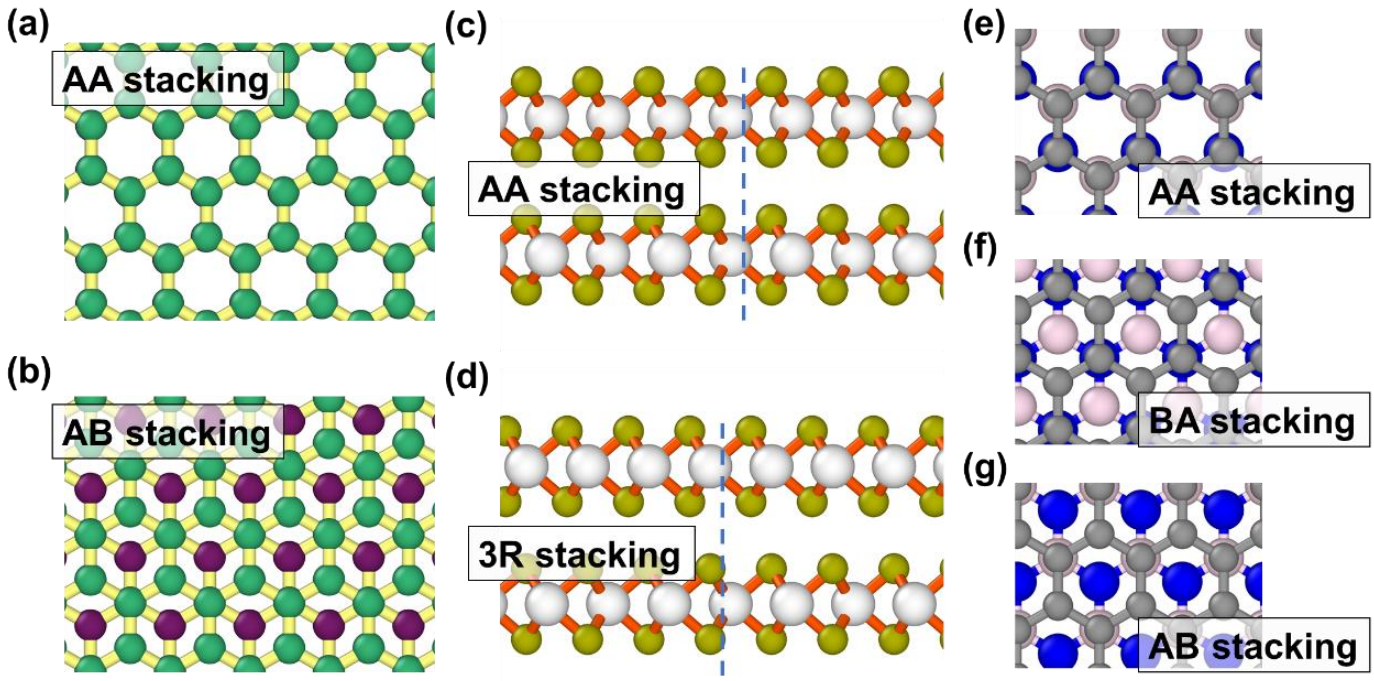

Figure S1. Illustration of stacking types for three materials. (a-b) Top view of AA and AB stacking of TBG. The covalent bonds among the top layer atom (green) and bottom layer atom (purple) are in yellow. (c-d) Side view of AA and 3R stacking of bilayer MoS_2 (yellow for S and white for Mo). (e-g) AA, BA and AB stacking of graphene on h-BN. The gray denotes carbon atoms, while pink denotes boron and blue denotes nitrogen.

For bilayer MoS_2, AA stacking domain is still high energy (Figure S1(c)) while 3R stacking (Figure S1(d)) corresponds to a low-energy configuration [4]. For graphene/h-BN structure, the situation becomes slightly more complicated. Three main stacking configurations are labeled. Following the notation of labeling stacking patterns from Ref [5, 6], the first one is labeled AA stacking (Figure S1(e)), meaning that all atoms sit on top of others. The second is labeled BA stacking (Figure S1(f)), meaning that a boron atom sits in the center of a graphene hexagon. The third is labeled AB stacking (Figure S1(g)), meaning that a nitrogen atom sits in the center of a graphene hexagon. It is reported that AB configuration is energetically most favorable with lowest interlayer distance [6, 7]. AA stacking and BA stacking have similar energies, and their interlayer distance is larger than that of AB stacking. In our calculation, we neglect the small energy difference between AA stacking and BA stacking [6] and treat them as the same.

To determine stable angle with initially imposed twist, the rotational axis is set to pass through the symmetric center of the triangular or hexagonal flake, where the initial stacking can be either AA stacking or AB(3R) stacking. We find that the preferred twisted state from either AA stacking or AB(3R) stacking is an objective physical state of both local rotational and translational energy minimum (See Sec.2, meaning that the flake will not undergo lateral translation during minimization), in agreement with earlier report [3]. For TBG and graphene/h-BN structures, we perform energy minimization using conjugate gradient (CG) algorithm. For the MoS_2 system, to acquire a more refined structure, we additionally employ the Hessian-free truncated Newton algorithm. Noted that for the center AB stacking, it is

challenging to achieve the local minimum energy states using static energy minimization methods. Thus, we adopt canonical (NVT) ensemble with Nose-Hoover thermostat, and calculate time-averaged twisted angle after stabilization. The dynamic simulation is performed at 1K. The final stable twist angle θ' is thus obtained after structural relaxation.

For forcefields, we have adopted Kolmogorov-Crespi interaction potential [8] to simulate interlayer interaction of graphene layers. The reactive empirical bond order (REBO) [9] potential is utilized to simulate intralayer carbon-carbon interaction. For graphene/h-BN heterostructure, we choose registry-dependent interlayer potential (ILP) [10] to simulate interlayer interaction between graphene and hexagonal boron nitride, while using REBO and tersoff [11] for intralayer interactions. As for twisted bilayer MoS_2 structures, the simulation is carried out with ReaxFF reactive force field [12].

2. Stability of Preferred Twisted States Against Translation

In this section, we demonstrate stability for preferred twisted states against lateral shifts using twisted bilayer graphene at $r = 30\sqrt{3}$ as an example. For initial AA stacking and AB stacking configuration of triangular and hexagonal shape, the translational energy landscapes of preferred twisted states, extracted from MD simulations, are presented at three stable angles, as a function of infinitesimal sliding in all directions [Figure S2]. The state at $(x, y) = (0,0)$ denotes the stable angle before any translation occurs. In each direction, the infinitesimal displacement is set as 0.001Å, then the energy minimization is performed at current translational state. The interlayer interaction energy (simulated by Kolmogorov-Crespi potential) is extracted at each lateral states. In the end, the obtained minimized energy values are gathered and plotted as translational energy landscape. It can be observed that translations in all directions result in increased energy, with the equilibrium twist angle already corresponding to the "valley" of energy.

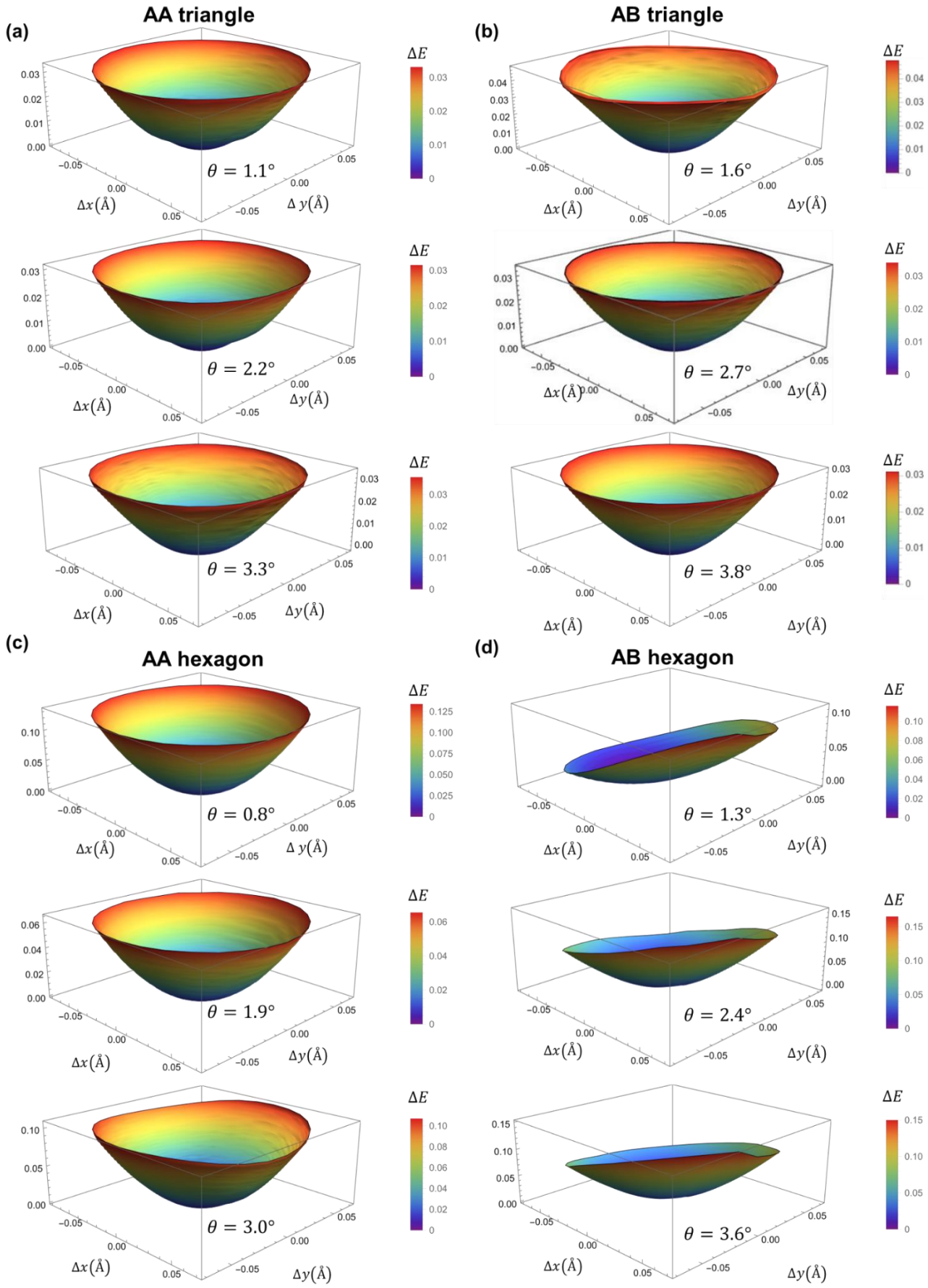

Figure S2. Translational energy landscape at three preferred twisted states for triangle and hexagon flakes for initial AA stacking and AB stacking. The calculation is performed for TBG with $r = 30\sqrt{3}$. It demonstrates that the preferred twisted states are at the local translational energy minimum.

3. More Details on Dimensionless Rotational Energy Landscape

3.1. Energy formula for identical bilayers considering moiré rotation

In the main text of Eqs.(1-4), the angle between the moiré vector and the lattice vector of the substrate is considered as $\pi/2$, in order to simplify the energy function results. Here, we present results considering moiré rotation (i.e., the angle is $(\pi+\theta)/2$).

For triangular flake with initial AA stacking,

$$\begin{aligned}S(\theta,r,p=1) = -\frac{3(1+2\cos\theta)\csc^3\frac{\theta}{2}\sec\frac{\theta}{2}}{32\pi^2r^2(1+2\cos 2\theta)}\{&-2\cos\left(\frac{4\pi r(-1+\cos\theta)}{\sqrt{3}}\sin\theta\right)\\ &+\cos\left[\frac{2}{3}\pi r\left(\sqrt{3}-\sqrt{3}\cos\theta+3\sin\theta\right)\right]\left(-\sqrt{3}+\sin\theta\right)\\ &+\cos\left[\frac{2}{3}\pi r\left(\sqrt{3}-\sqrt{3}\cos\theta-3\sin\theta\right)\right]\left(\sqrt{3}+\sin\theta\right)\\ &+2\sqrt{3}\cos\theta\sin\left(\frac{2\pi r(-1+\cos\theta)}{\sqrt{3}}\right)\sin(2\pi r\sin\theta)\}.\end{aligned} \quad (S1)$$

For triangle flake with initial AB stacking,

$$\begin{aligned}S(\theta,r,p=1) = &\frac{1}{16\pi^2r^2(1+2\cos 2\theta)}\cdot 3\csc^2\frac{\theta}{2}\sin\frac{3\theta}{2}\\ &(\cos\left[\frac{1}{3}\pi\left(1-2\sqrt{3}r+2\sqrt{3}r\cos\theta+6r\sin\theta\right)\right]\left(\csc\frac{\theta}{2}+\sqrt{3}\sec\frac{\theta}{2}\right)\\ &-2\csc\frac{\theta}{2}\sin\left[\frac{1}{6}\pi\left(1+8\sqrt{3}r(-1+\cos\theta)\right)\right]\\ &+\left(\csc\frac{\theta}{2}-\sqrt{3}\sec\frac{\theta}{2}\right)\sin\left\{\frac{1}{6}\pi\left[1-4\sqrt{3}r\cos\theta+4r\left(\sqrt{3}+3\sin\theta\right)\right]\right\})\end{aligned} \quad (S2)$$

For hexagon flake with initial AA stacking,

$$\begin{aligned}S(\theta,r,p=1) = &\frac{3\csc^2\frac{\theta}{2}}{8\pi^2r^2[1+2\cos(2\theta)]}\cdot\{-(-1+2\cos\theta)\\ &\left[\cos\left(2\pi r\cos\frac{\theta}{2}\sqrt{2-2\cos\theta}\right)\cos\left(\frac{2}{3}\pi r\sqrt{6-6\cos\theta}\,\sin\frac{\theta}{2}\right)-\cos\left(\frac{4}{3}\pi r\sqrt{6-6\cos\theta}\,sin\frac{\theta}{2}\right)\right]\\ &+\sqrt{3}\cos\frac{3\theta}{2}\csc\frac{\theta}{2}\sin\left(2\pi r\cos\frac{\theta}{2}\sqrt{2-2\cos\theta}\right)\sin\left(2\sqrt{\frac{2}{3}}\pi r\sqrt{1-\cos\theta}\sin\frac{\theta}{2}\right)\}.\end{aligned} \quad (S3)$$

For hexagon flake with initial AB stacking,

$$S(\theta,r,p=1)=\frac{3\sqrt{3}\csc\frac{\theta}{4}\csc^2\frac{\theta}{2}\sec\frac{\theta}{4}\sec\frac{\theta}{2}}{256\pi^2r^2[1+2\cos(2\theta)]\left(-3+\sqrt{3}\cot\frac{\theta}{2}\right)}\cdot$$
$$\left[-8\cos\left(\frac{3\theta}{2}\right)\cos\left(\frac{4}{3}\pi r\sqrt{6-6\cos\theta}\sin\frac{\theta}{2}\right)\left(\cos\frac{\theta}{2}-\sqrt{3}\sin\frac{\theta}{2}\right)\right.$$
$$-4\cos\left(\frac{2}{3}\pi r\sqrt{6-6\cos\theta}\sin\frac{\theta}{2}\right)\left(\cos\frac{\theta}{2}-\sqrt{3}\sin\frac{\theta}{2}\right)$$
$$\cdot\left[\left(2\cos\frac{\theta}{2}-\cos\frac{3\theta}{2}\right)\cos\left(2\pi r\cos\frac{\theta}{2}\sqrt{2-2\cos\theta}\right)-3\sin\frac{3\theta}{2}\sin\left(2\pi r\cos\frac{\theta}{2}\sqrt{2-2\cos\theta}\right)\right]$$
$$+\csc\frac{\theta}{4}\sec\frac{\theta}{4}\left(\sqrt{3}\cos\frac{\theta}{2}-3\sin\frac{\theta}{2}\right)\{-\cos\left(2\pi r\cos\frac{\theta}{2}\sqrt{2-2\cos\theta}\right)[\sin\theta+\sin(2\theta)]$$
$$-(3\cos\theta+\cos2\theta)\sin\left(2\pi r\cos\frac{\theta}{2}\sqrt{2-2\cos\theta}\right)\}\sin\left(2\sqrt{\frac{2}{3}}\pi r\sqrt{1-\cos\theta}\sin\frac{\theta}{2}\right)$$
$$-2(1+2\cos\theta)((2-4\cos\theta)\cos\left\{\frac{1}{3}\left[\pi+2\pi r\sqrt{2-2\cos\theta}\left(3\cos\frac{\theta}{2}-\sqrt{3}\sin\frac{\theta}{2}\right)\right]\right\}$$
$$\left.+2\left(-2+\cos\theta+\sqrt{3}\sin\theta\right)\sin\left\{\frac{1}{6}\left[\pi+4\pi r\sqrt{2-2\cos\theta}\left(3\cos\frac{\theta}{2}+\sqrt{3}\sin\frac{\theta}{2}\right)\right]\right\}\right)]. \qquad (S4)$$

Figure S3 depict the three-dimensional plot of the total energy function Eqs. (1-4) for triangular and hexagonal flake with initial AA and AB stacking. Some troughs can be observed on the surface, indicating the presence of local energy minima. Therefore, the energy function can be used to determine stable twist angles for a given flake size r, as illustrated in Figure 3. Noted that the 3-D plot of Eqs. S(1-4) are almost identical with Eqs. (1-4).

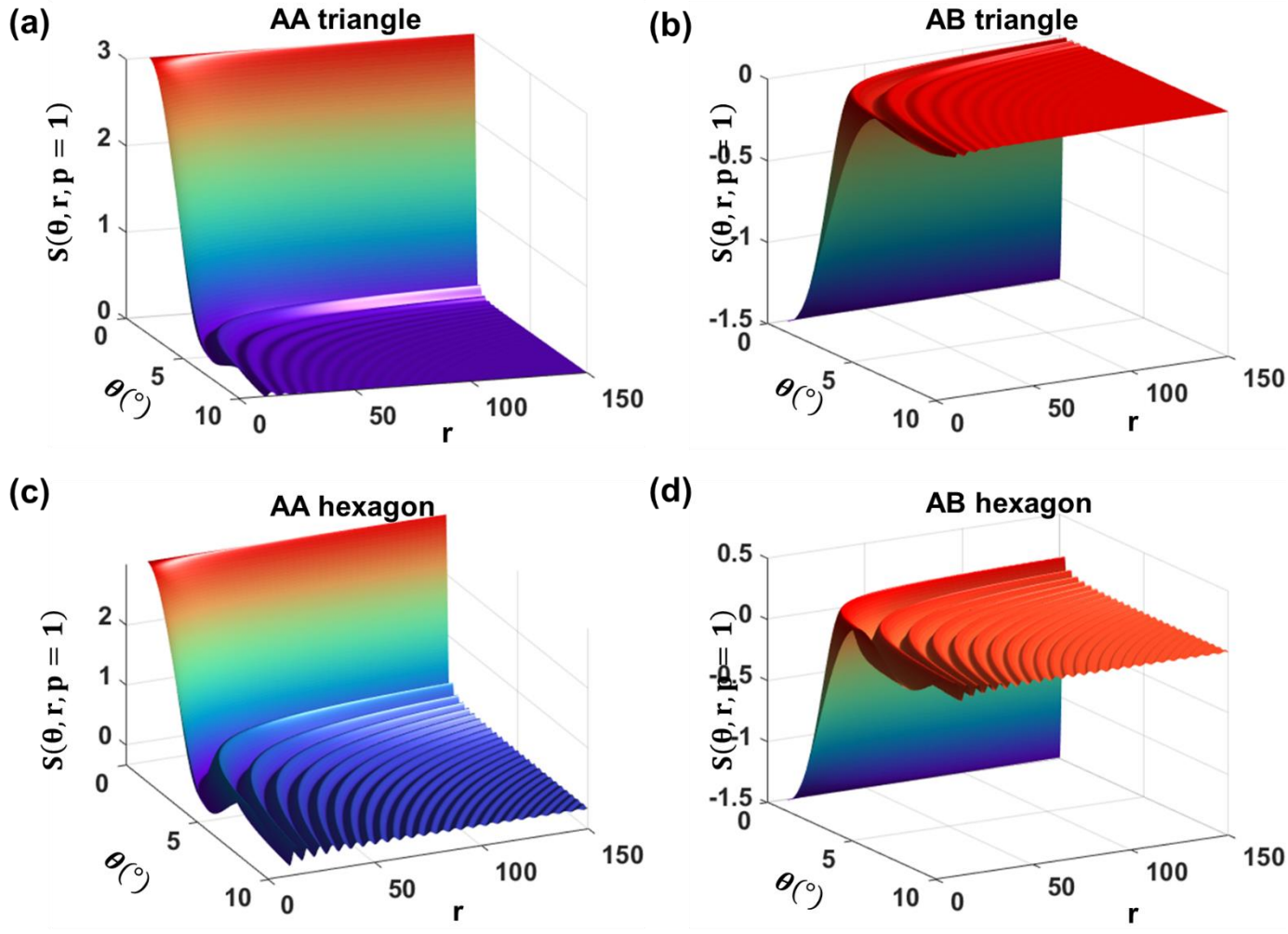

Figure S3. Surface plot of total energy function $S(\theta,r,p=1)$ for (a) Eq.1 (b) Eq.2 (c) Eq.3 (d) Eq.4, as labeled in main text.

We also tested the local energy minimum twist angles for Eqs. S(1-4), which closely align with the simplified form of Eqs. (1-4). This dedicates that the simplification of moiré rotation will not affect our results.

3.2. Energy formula for graphene/h-BN

For hexagonal graphene/h-BN heterostructures, the total energy function with initial AA stacking is (based on $\rho' = -\sum_{\vec{G}} \cos\left(\vec{G}\cdot\vec{r}\right)$ and substituting $p = 0.98$ [13])

$$
\begin{aligned}
S(\theta,r,p) = {} & \frac{-\sqrt{3}}{8\pi^2 r^2(1+p^2-2p\cos\theta)(-1+2\cos(2A^-)} \cdot \\
& \{2\sqrt{3}\cos\left[\frac{\pi}{3}(1+2C\cos A^-)\right] - \sqrt{3}\cos\left[\frac{\pi}{3}\left(1+C\cos A^- + \sqrt{3}C\sin A^-\right)\right] + \\
& 2\sqrt{3}\sin\left[\frac{\pi}{6}(1+4C\cos A^-)\right] - \sqrt{3}\sin\left[\frac{\pi}{6}\left(1+2C\cos A^- - 2\sqrt{3}C\sin A^-\right)\right] \\
& -\sqrt{3}\sin\left[\frac{\pi}{6}\left(1+2C\cos A^- + 2\sqrt{3}C\sin A^-\right)\right] - \cos\left[\frac{\pi}{3}\left(1+C\cos A^- + \sqrt{3}C\sin A^-\right)\right]\tan A^- \\
& -4\cos\left(\frac{\pi}{6}+\frac{\pi C}{\sqrt{3}}\sin A^-\right)\sin\left(\frac{\pi C\cos A^-}{3}\right)\tan A^- + \sin\left[\frac{\pi}{6}\left(1+2C\cos A^- - 2\sqrt{3}C\sin A^-\right)\right]\tan A^- \\
& +4\sin\left(\frac{\pi\, C\cos A^-}{3}\right)\sin\left[\frac{\pi}{3}\left(1+\sqrt{3}C\sin A^-\right)\right]\tan A^- - \sin\left[\frac{\pi}{6}\left(1+2C\cos A^- + 2\sqrt{3}C\sin A^-\right)\right]\tan A^- \\
& +\cos\left[\frac{\pi}{3}\left(1+C\cos A^- - \sqrt{3}C\sin A^-\right)\right]\left(-\sqrt{3}+\tan A^-\right)\}. \qquad (S5)
\end{aligned}
$$

The definitions of the symbols in above equations are listed as follows.

$$A^- = \theta - \arccos\left(\frac{-p+\cos\theta}{\sqrt{1+p^2-2p\cos\theta}}\right),$$

$$A^+ = \theta + \arccos\left(\frac{-p+\cos\theta}{\sqrt{1+p^2-2p\cos\theta}}\right),$$

$$B^- = \theta - \arcsin\left(\frac{-p+\cos\theta}{\sqrt{1+p^2-2p\cos\theta}}\right)$$

$$B^+ = \theta + \arcsin\left(\frac{-p+\cos\theta}{\sqrt{1+p^2-2p\cos\theta}}\right)$$

$$C = 2\sqrt{3}r\sqrt{1+p^2-2p\cos\theta}.$$

The total energy function of hexagonal graphene/h-BN flakes with initial AB stacking is (based on $\rho' = -\sum_{\vec{G}} \cos\left(\vec{G}\cdot\vec{r}\right)$ and substituting $p = 0.98$),

$$
\begin{aligned}
S(\theta,r,p) = {} & -\frac{-1+3\tan^2 A^-}{H}\cdot\{6\sqrt{3}[1+2\cos(2B^+)]\cos(2C) - 3\sqrt{3}\cos D^+ \\
& -6\sqrt{3}\cos(2B^+)\cos D^+ - \sqrt{3}\sin(E)\,F - 2\sqrt{3}\cos(2B^+)\sin(E)\,F \\
& -3\cot B^+\sin(E)\,F + 6\cos(2A^-)\cot B^+\sin(E)\,F + 6\csc B^+\sin A^-\sin(E)\,F \\
& +12\cos 2B^+\csc B^+\sin A^-\sin(E)\,F + \sqrt{3}\sin(C)\sin G \\
& +2\sqrt{3}\cos 2B^+\sin C\sin G - 3\cos D^+\tan A^- - 6\cos 2B^+\cos D \\
& \tan A^- + 3\sin C\sin G\tan A^- + 6\cos(2B^+)\sin C\sin G\tan A^- \\
& +3(1+2\cos(2B^+))\cos D^-\left(-\sqrt{3}+\tan A^-\right)]\}. \qquad (S6)
\end{aligned}
$$

The definitions of the symbols in above equations are listed as follows,

$$A^- = \theta - \arccos\left(\frac{-p+\cos\theta}{\sqrt{1+p^2-2p\cos\theta}}\right),$$

$$A^+ = \theta + \arccos\left(\frac{-p+\cos\theta}{\sqrt{1+p^2-2p\cos\theta}}\right),$$

$$B^- = \theta - \arcsin\left(\frac{-p + \cos\theta}{\sqrt{1 + p^2 - 2p\cos\theta}}\right)$$

$$B^+ = \theta + \arcsin\left(\frac{-p + \cos\theta}{\sqrt{1 + p^2 - 2p\cos\theta}}\right)$$

$$C = \frac{2\pi r\sqrt{1 + p^2 - 2p\cos\theta}\cdot\cos A^-}{\sqrt{3}},$$

$$D^- = \frac{2}{3}\pi r\sqrt{1 + p^2 - 2p\cos\theta}\left(\sqrt{3}\cos A^- - 3\sin A^-\right)$$

$$D^+ = \frac{2}{3}\pi r\sqrt{1 + p^2 - 2p\cos\theta}\left(\sqrt{3}\cos A^- + 3\sin A^-\right)$$

$$E = \frac{2\pi r(-1 + p\cos\theta)}{\sqrt{3}}$$

$$F = \sin(2p\pi r\sin\theta)$$

$$G = 2\pi r\sqrt{1 + p^2 - 2p\cos\theta}\cdot\sin A^-.$$

$$\mathrm{H} = 4\sqrt{3}\pi^2 r^2(1 + p^2 - 2p\cos\theta)(-1 + 2\cos 2A^-)\,(1 + 2\cos 2B^+)\,(-1 + 3(\tan A^-)^2)$$

Substitute the corresponding variables into the equation yields the full expression for the formula.

In Fig. S4 we demonstrate the three-dimensional plot of the total energy function for graphene/h-BN, similar troughs can be observed on the surface.

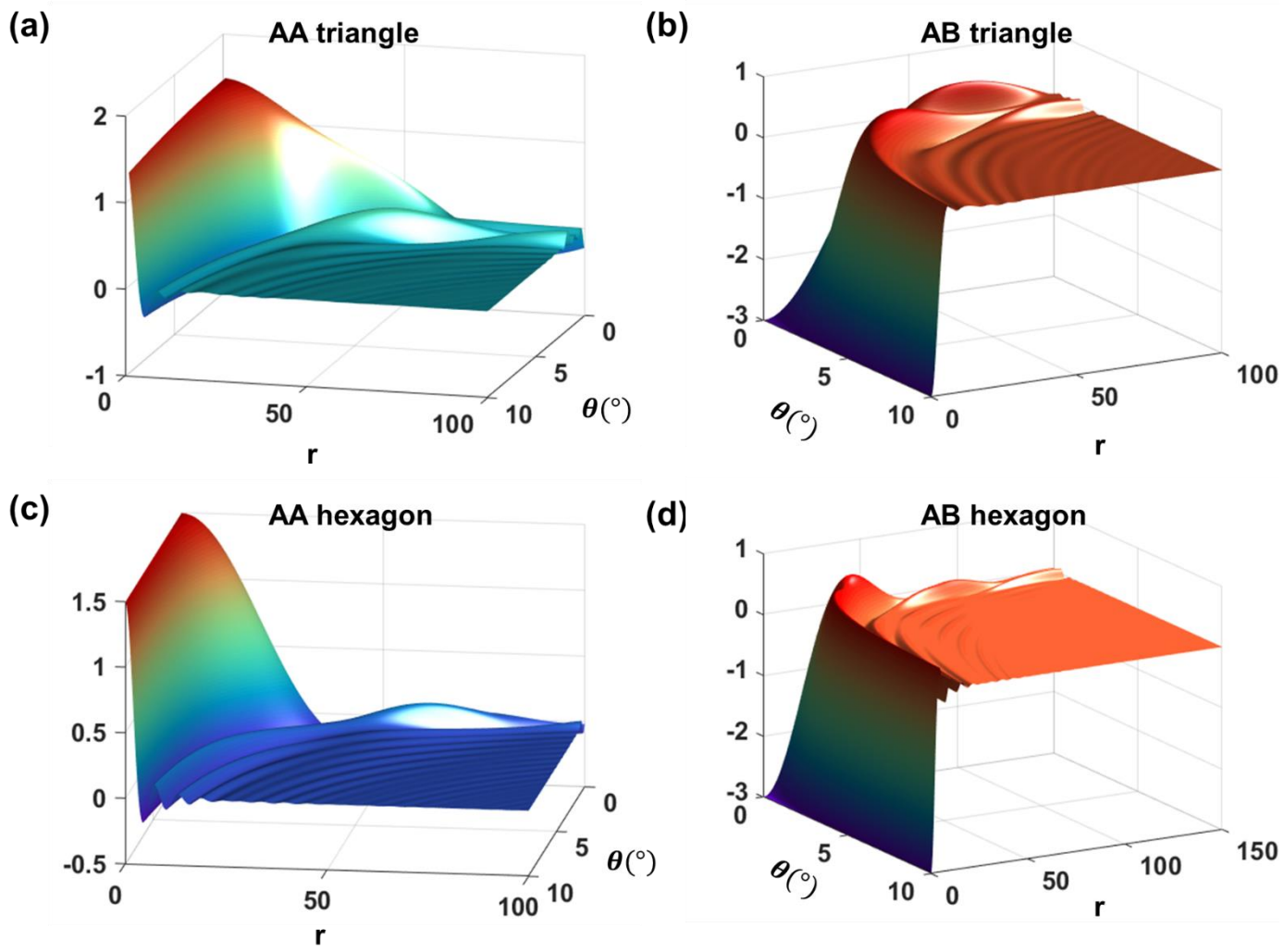

Figure S4. Surface plot of total energy function $S(\theta, r, p = 1)$ for graphene/h-BN system.

3.3. Energy formula for $\rho = \sum_{\vec{G}} cos\left(\vec{G} \cdot \vec{r}\right)$

Here we present total energy function for heterostructures based on $\rho = \sum_{\vec{G}} cos\left(\vec{G} \cdot \vec{r}\right)$, which could be resulted by strain engineering of TBG [14]. The mismatch parameter p tunes the strain-engineering amplitude.

Energy function of triangular flake with initial AA stacking is,

$$S(\theta, r, p) = \frac{3}{D} \cdot [\, 2\cos(C\cos A)\cos\left(\frac{C\sin A}{\sqrt{3}}\right) - 2\cos\left(\frac{2C\sin A}{\sqrt{3}}\right) + \sqrt{3}\csc\left(\frac{1}{2}B\right)\sec\left(\frac{1}{2}B\right)\sin A\sin(C\cos A)\sin\left(\frac{2C\sin A}{\sqrt{3}}\right)]. \quad \text{(S7)}$$

The definitions of the symbols in above equations are listed as follows.

$$A = \theta + \arcsin\left(\frac{-p + \cos\theta}{\sqrt{1 + p^2 - 2p\cos\theta}}\right),$$

$$B = -\theta + \arccos\left(\frac{-p + \cos\theta}{\sqrt{1 + p^2 - 2p\cos\theta}}\right),$$

$$C = 2\pi r\sqrt{1 + p^2 - 2p\cos\theta},$$

$$D = 4\pi^2 r^2 (1 + p^2 - 2p\cos\theta)(1 - 2\cos(2A)).$$

Energy function of triangular flake with initial AB stacking is,

$$S(\theta,r,p)=\frac{9\csc^3 A}{D}\cdot[2\cos\left(\frac{\pi}{6}+A-2B\right)-2\cos\left(\frac{\pi}{6}-A-2B\right)$$
$$-\cos\left(\frac{\pi}{6}+A+B-C\right)+\cos\left(\frac{\pi}{6}-A+B-C\right)-\cos\left(\frac{\pi}{6}+A+B+C\right)$$
$$+\cos\left(\frac{\pi}{6}-A+B+C\right)+\sqrt{3}\sin\left(\frac{\pi}{6}+A+B-C\right)+\sqrt{3}\sin\left(\frac{\pi}{6}-A+B-C\right)$$
$$-\sqrt{3}\sin\left(\frac{\pi}{6}+A+B+C\right)-\sqrt{3}\sin\left(\frac{\pi}{6}-A+B+C\right)]. \quad (S8)$$

The definitions of the symbols in above equations are listed as follows.

$$A=\theta-\arccos\left(\frac{-p+\cos\theta}{\sqrt{1+p^2-2p\cos\theta}}\right),$$

$$B=\frac{2\pi r\sqrt{1+p^2-2p\cos\theta}\cdot\cos A}{\sqrt{3}},$$

$$C=2\pi r\sqrt{1+p^2-2p\cos\theta}\cdot\sin A,$$

$$D=8\pi^2r^2(1+p^2-2p\cos\theta)(3-9\cot^2 A).$$

Energy function of hexagonal flake with initial AA stacking is,

$$S(\theta,r,p)=\frac{-1+3\tan^2 A^-}{H}\cdot\{6\sqrt{3}[1+2\cos(2B^+)]\cos(2C)\ -3\sqrt{3}\cos D^+$$
$$-6\sqrt{3}\cos(2B^+)\cos D^+-\sqrt{3}\sin(E)\,F-2\sqrt{3}\cos(2B^+)\sin(E)\,F$$
$$-3\cot B^+\sin(E)\,F+6\cos(2A^-)\cot B^+\sin(E)\,F+6\csc B^+\sin A^-\sin(E)\,F$$
$$+12\cos 2B^+\csc B^+\sin A^-\sin(E)\,F+\sqrt{3}\sin(C)\sin G$$
$$+2\sqrt{3}\cos 2B^+\sin C\sin G-3\cos D^+\tan A^--6\cos 2B^+\cos D$$
$$\tan A^-+3\sin C\sin G\tan A^-+6\cos(2B^+)\sin C\sin G\tan A^-$$
$$+3(1+2\cos(2B^+))\cos D^-\left(-\sqrt{3}+\tan A^-\right)]\}. \quad (S9)$$

The definitions of the symbols in above equations are listed as follows,

$$A^-=\theta-\arccos\left(\frac{-p+\cos\theta}{\sqrt{1+p^2-2p\cos\theta}}\right),$$

$$A^+=\theta+\arccos\left(\frac{-p+\cos\theta}{\sqrt{1+p^2-2p\cos\theta}}\right),$$

$$B^-=\theta-\arcsin\left(\frac{-p+\cos\theta}{\sqrt{1+p^2-2p\cos\theta}}\right)$$

$$B^+=\theta+\arcsin\left(\frac{-p+\cos\theta}{\sqrt{1+p^2-2p\cos\theta}}\right)$$

$$C=\frac{2\pi r\sqrt{1+p^2-2p\cos\theta}\cdot\cos A^-}{\sqrt{3}},$$

$$D^-=\frac{2}{3}\pi r\sqrt{1+p^2-2p\cos\theta}\left(\sqrt{3}\cos A^--3\sin A^-\right)$$

$$D^+=\frac{2}{3}\pi r\sqrt{1+p^2-2p\cos\theta}\left(\sqrt{3}\cos A^-+3\sin A^-\right)$$

$$E=\frac{2\pi r(-1+p\cos\theta)}{\sqrt{3}}$$

$$F=\sin(2p\pi r\sin\theta)$$

$$G = 2\pi r\sqrt{1+p^2-2p\cos\theta}\cdot\sin A^-.$$

$$\mathrm{H} = 4\sqrt{3}\pi^2 r^2(1+p^2-2p\cos\theta)(-1+2\cos 2A^-)\,(1+2\cos 2B^+)\,(-1+3(\tan A^-)^2)$$

Energy function of hexagonal flake with initial AB stacking is,

$$\begin{aligned}S(\theta,r,p) = {} & \frac{\sqrt{3}}{8\pi^2 r^2(1+p^2-2p\cos\theta)(-1+2\cos(2A^-)}\cdot \\ & \{2\sqrt{3}\cos\left[\frac{\pi}{3}(1+2C\cos A^-)\right]-\sqrt{3}\cos\left[\frac{\pi}{3}\left(1+C\cos A^-+\sqrt{3}C\sin A^-\right)\right]+ \\ & 2\sqrt{3}\sin\left[\frac{\pi}{6}(1+4C\cos A^-)\right]-\sqrt{3}\sin\left[\frac{\pi}{6}\left(1+2C\cos A^--2\sqrt{3}C\sin A^-\right)\right] \\ & -\sqrt{3}\sin\left[\frac{\pi}{6}\left(1+2C\cos A^-+2\sqrt{3}C\sin A^-\right)\right]-\cos\left[\frac{\pi}{3}\left(1+C\cos A^-+\sqrt{3}C\sin A^-\right)\right]\tan A^- \\ & -4\cos\left(\frac{\pi}{6}+\frac{\pi C}{\sqrt{3}}\sin A^-\right)\sin\left(\frac{\pi C\cos A^-}{3}\right)\tan A^-+\sin\left[\frac{\pi}{6}\left(1+2C\cos A^--2\sqrt{3}C\sin A^-\right)\right]\tan A^- \\ & +4\sin\left(\frac{\pi\,C\cos A^-}{3}\right)\sin\left[\frac{\pi}{3}\left(1+\sqrt{3}C\sin A^-\right)\right]\tan A^--\sin\left[\frac{\pi}{6}\left(1+2C\cos A^-+2\sqrt{3}C\sin A^-\right)\right]\tan A^- \\ & +\cos\left[\frac{\pi}{3}\left(1+C\cos A^--\sqrt{3}C\sin A^-\right)\right]\left(-\sqrt{3}+\tan A^-\right)\}. \qquad (S10)\end{aligned}$$

The definitions of the symbols in above equations are listed as follows.

$$A^- = \theta - \arccos\left(\frac{-p+\cos\theta}{\sqrt{1+p^2-2p\cos\theta}}\right),$$

$$A^+ = \theta + \arccos\left(\frac{-p+\cos\theta}{\sqrt{1+p^2-2p\cos\theta}}\right),$$

$$B^- = \theta - \arcsin\left(\frac{-p+\cos\theta}{\sqrt{1+p^2-2p\cos\theta}}\right)$$

$$B^+ = \theta + \arcsin\left(\frac{-p+\cos\theta}{\sqrt{1+p^2-2p\cos\theta}}\right)$$

$$C = 2\sqrt{3}r\sqrt{1+p^2-2p\cos\theta}.$$

3.4. Energy formula for zero-twist bilayers with varying lattice mismatch

Moiré pattern purely caused by lattice mismatch strain can be commonly observed where different 2D materials are stacked with crystal axis aligned [15], or identical bilayers imposed by biaxial strain engineering [16]. In this case, the rotation angle $\theta = 0°$. These energy formulas based on $\rho = \sum_{\vec{G}} cos\left(\vec{G}\cdot\vec{r}\right)$ are presented as follows.

The total energy function for triangle flake with initial AA stacking is

$$S(\theta=0,r,p)=\frac{\sin\left[\frac{(-1+p)\pi r}{\sqrt{3}}\right]\left\{6(-1+p)\pi r\cos\left[\frac{(-1+p)\pi r}{\sqrt{3}}\right]+\sqrt{3}\sin\left[\sqrt{3}(-1+p)\pi r\right]\right\}}{\sqrt{3}(-1+p)^2\pi^2r^2}. \quad \text{(S11)}$$

The total energy function for triangle flake with initial AB stacking is

$$\begin{aligned}S(\theta=0,r,p)=&\frac{1}{4\sqrt{3}(-1+p)^2\pi^2r^2}\cdot\\&(\sqrt{3}[-1+6(-1+p)\pi r]\cos\left[\frac{2(-1+p)\pi r}{\sqrt{3}}\right]+\sqrt{3}\cos\left[\frac{4(-1+p)\pi r}{\sqrt{3}}\right]\\&-3\left\{1+2(-1+p)\pi r+2\cos\left[\frac{2(-1+p)\pi r}{\sqrt{3}}\right]\right\}\sin\left[\frac{2(-1+p)\pi r}{\sqrt{3}}\right]).\end{aligned} \quad \text{(S12)}$$

The total energy function for hexagon flake with initial AA stacking is

$$S(\theta=0,r,p)=\frac{3\left\{1+2\cos\left[\frac{2(-1+p)\pi r}{\sqrt{3}}\right]\right\}\sin^2\left[\frac{(-1+p)\pi r}{\sqrt{3}}\right]}{(-1+p)^2\pi^2r^2}. \quad \text{(S13)}$$

The total energy function for hexagon flake with initial AB stacking is

$$S(\theta=0,r,p)=\frac{3\left\{-\cos\left[\frac{2(-1+p)\pi r}{\sqrt{3}}\right]+\cos\left[\frac{4(-1+p)\pi r}{\sqrt{3}}\right]\right\}}{4(-1+p)^2\pi^2r^2}. \quad \text{(S14)}$$

3.5. Energy formula considering local relaxation

In this section, we will discuss the effect of varying degree of local relaxation (i.e., the on-site shrinkage of high-energy domain relaxation). For small rotation angle, AB regions tend to expand and AA regions shrink to become solitons [17]. The relaxed pattern displays a network of SP regions connecting AA regions, forming domain walls surrounding AB regions [18, 19]. In relatively large twist angles, the appearance of SP region is suppressed.

We propose a general form of energy density function $\rho=\sum_{n=1}^{\infty}a_n\sum_{\vec{G}}\cos(n\vec{G}\cdot\vec{r})$. For initial AA stacking, we can use $\rho=\sum_{n=1}^{\infty}a_n\left[\cos\left(\frac{4\pi nx}{\sqrt{3}\lambda}\right)+2\cos\left(\frac{2\pi x}{\sqrt{3}\lambda}\right)\cos\left(\frac{2\pi y}{\lambda}\right)\right]$. For initial AB stacking, we can use $\rho=\sum_{n=1}^{\infty}a_n\left\{\cos\left[\frac{4\pi n\left(x-\frac{\lambda}{\sqrt{3}}\right)}{\sqrt{3}\lambda}\right]+2\cos\left[\frac{2\pi n\left(x-\frac{\lambda}{\sqrt{3}}\right)}{\sqrt{3}\lambda}\right]\cos\left(\frac{2\pi ny}{\lambda}\right)\right\}$. By choosing appropriate parameter a_n, the density function can capture moiré patterns under varying degrees of structural relaxation. The previous discussion without consideration

of relaxation corresponds to $a_1 = 1$ and $a_n = 0$ $(n > 2)$, taking the form of only the first item as $\sum_{\vec{G}} \cos\left(\vec{G} \cdot \vec{r}\right)$.

To apply the density function in practice, a finite number of terms can be utilized. The undetermined coefficients, a_n, can be determined by imposing constraints on the relative flatness of AB and the peak width of AA. A wide range of coefficients can be theoretically employed provided that the fundamental moiré geometric criteria are adequately satisfied. We use a few for demonstration in Fig. S5(a).

In Fig. S5, we present moiré patterns using the general form of energy density function using different number of terms. It is observable that as the number of terms increases, the degree of local relaxation progressively intensifies. Initial AA stacking flake with $r = 30\sqrt{3}$, $\theta = 2°$ is adopted for illustration, and refer to legends in Fig. S5 for specific coefficients a_n. The calculation follows similar approach in Eqs. (1-4).

The total energy function considering local relaxation for triangle flake with initial AA stacking is

$$S(\theta, r, p = 1) = \sum\nolimits_n a_n \frac{-3\sin^2\left(n\pi r\sqrt{2 - 2\cos\theta}\right)}{2n^2\pi^2 r^2(-1 + 2\cos\theta)}. \quad (S15)$$

The total energy function considering local relaxation for triangle flake with initial AB stacking is

$$S(\theta, r, p = 1) = \sum\nolimits_n a_n \frac{-\left(2\cos\frac{2n\pi}{3} + \cos\frac{4n\pi}{3}\right)\sin^2\left(n\pi r\sqrt{2 - 2\cos\theta}\right)}{2n^2\pi^2 r^2(-1 + 2\cos\theta)}. \quad (S16)$$

The total energy function considering local relaxation for hexagon flake with initial AA stacking is

$$S(\theta, r, p = 1) = \sum\nolimits_n a_n \frac{\sqrt{1 - \cos\theta}\sin^2\left(n\pi r\sqrt{2 - 2\cos\theta}\right) + 2\sqrt{2}n\pi r\sin^2\frac{\theta}{2}\sin\left(2n\pi r\sqrt{2 - 2\cos\theta}\right)}{2n^2\pi^2 r^2(-1 + 2\cos\theta)^{\frac{3}{2}}}. \quad (S17)$$

The total energy function considering local relaxation for hexagon flake with initial AB stacking is

$$\begin{aligned} S(\theta, r, p = 1) = \sum\nolimits_n \frac{a_n}{-6n^2\pi^2 r^2(-1 + \cos\theta)} \Big(&2\cos\frac{2n\pi}{3} \\ &+ \cos\frac{4n\pi}{3}\Big)\sin\left(n\pi r\sqrt{2 - 2\cos\theta}\right)\left[2n\pi r\sqrt{2 - 2\cos\theta}\cos\left(n\pi r\sqrt{2 - 2\cos\theta}\right)\right. \\ &\left. + \sin\left(n\pi r\sqrt{2 - 2\cos\theta}\right)\right]. \end{aligned} \quad (S18)$$

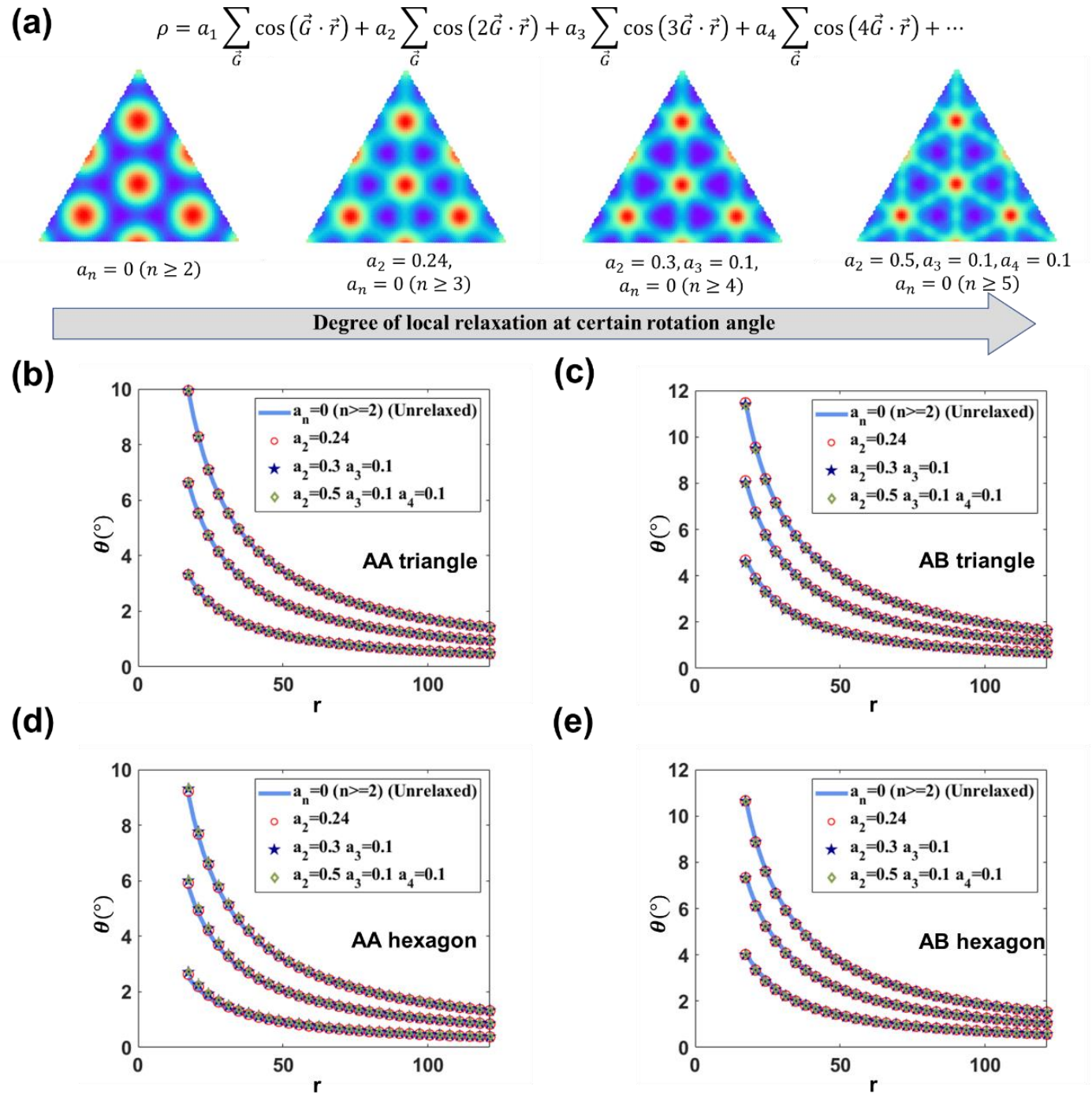

FIG. S5. Application of general energy density function for structural relaxation. (a) Illustration on modeling varying degree of local relaxation using different number of terms and proper coefficients a_n. More terms intensify relaxation effects. (b-d) Comparison of the results for the first three angles of local minimum from multi-term energy density functions (see legends). Results are for triangular flake with initial AA stacking (a), AB stacking (b), and hexagonal flake with initial AA stacking (c), AB stacking (d).

Using these multi-term energy density functions, we can compute the first three angels of local energy minima for each size *r*, and compare with those obtained from single-term energy density function (i.e., unrelaxed, Eqs. (1-4)). The comparisons for triangle flakes of different initial stackings show excellent agreement [Fig. S5(b-e)]. The conclusions are the same for hexagonal flakes. Therefore, our analytical theory shows that local relaxation does not practically affect

angles of local energy extrema. This conclusion is consistent with earlier works where the SP region is modeled with even simpler rectangular stripes [20] mimicking dislocation lines with finite width. It is found that the width of the stripe does not change the angles of local energy extrema produced from unrelaxed pattern [20].

3.6. Energy formula for square shapes

Using our analytical approach, integrations of certain polygon shapes can be explicitly evaluated. Here, we present the total energy functions for square flakes with diagonal length of $\sqrt{2}r$. The results for identical bilayers are shown, still assuming moiré vector and the lattice vector are perpendicular.

For squares with initial AA stacking,

$$S(\theta, r, p = 1) = \frac{\sqrt{3}\left[\csc^2\left(\frac{\theta}{2}\right)\sin 2\pi r\sqrt{1-\cos\theta}\sin\frac{2\pi r\sqrt{1-\cos\theta}}{\sqrt{3}} + \frac{\pi r\sin\frac{4\pi r\sqrt{1-\cos\theta}}{\sqrt{3}}}{\sqrt{1-\cos\theta}}\right]}{2\pi^2 r^2} \quad (S19)$$

For squares with initial AB stacking,

$$S(\theta, r, p = 1) = -\frac{\sqrt{3}\left[\csc^2\left(\frac{\theta}{2}\right)\sin 2\pi r\sqrt{1-\cos\theta}\sin\frac{2\pi r\sqrt{1-\cos\theta}}{\sqrt{3}} + \frac{\pi r\sin\frac{4\pi r\sqrt{1-\cos\theta}}{\sqrt{3}}}{\sqrt{1-\cos\theta}}\right]}{4\pi^2 r^2} \quad (S20)$$

4. Scaling Performance on Interlayer Rotational Torque

Here we demonstrate more results for the universal scaling laws on interlayer rotational torque. Main text Figure 4 shows that there is excellent scaling agreement for both triangular and hexagonal TBG flakes with initial AA and AB stacking configuration with the fixed r. Here, we show that for the same flake shape with identical initial stacking configuration (e.g. TBG triangular shape with initial AA stacking), coefficient *K* exhibits negligible variation with varying r for a particular simulation potential [Fig. S6]. Both Kolmogorov-Crespi interaction potential and registry-dependent interlayer potential [10] (ILP) lead to the same observation regarding the constant of *K*. The dependence of K on simulation potential is reasonable. These results demonstrate the robustness of the scaling performance of our results.

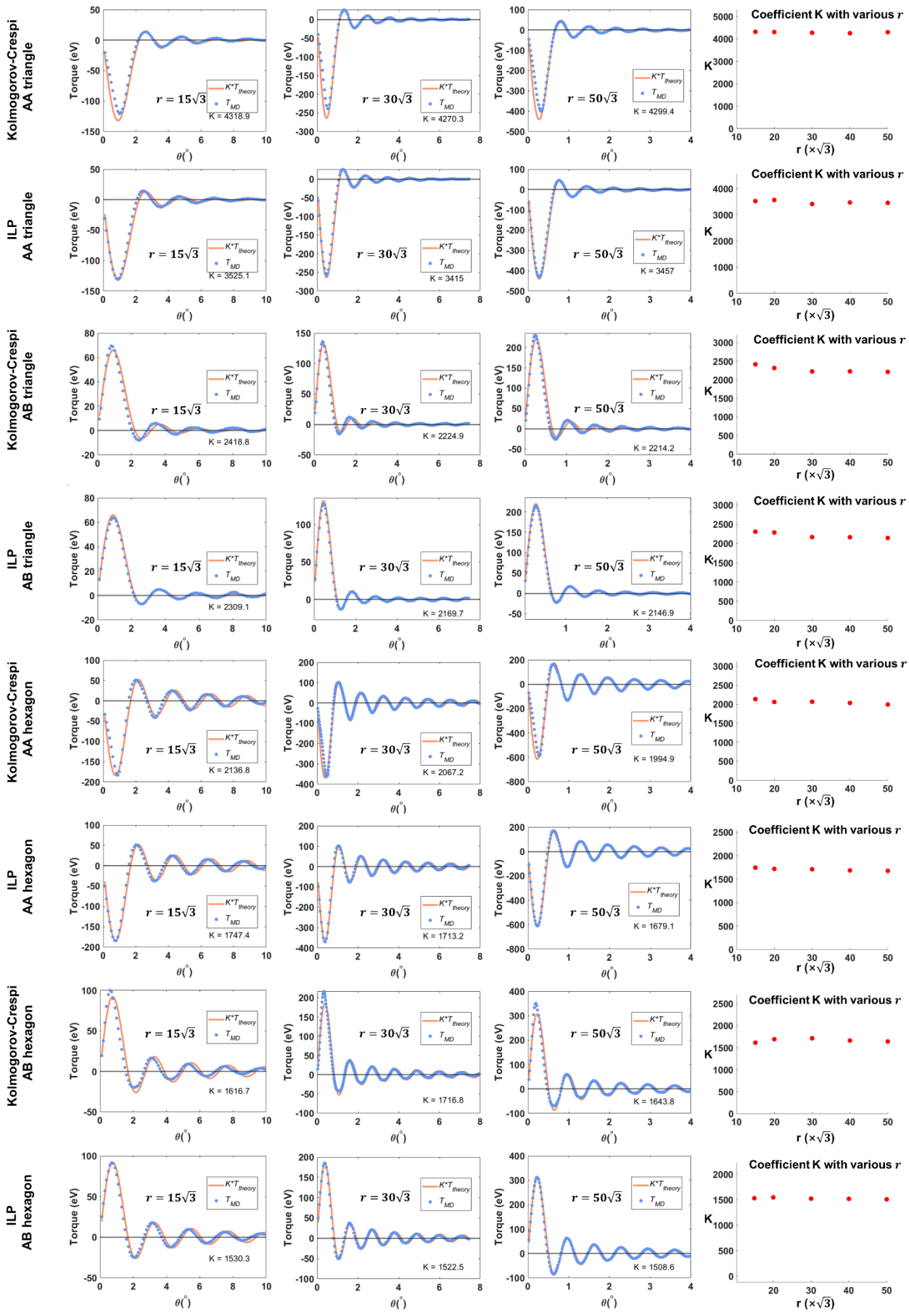

FIG. S6. For each flake shape and different size parameter r, the theoretically calculated interlayer torque and simulation results are shown. The simulation results using Kolmogorov-Crespi interaction potential and registry-dependent interlayer potential (ILP) are also compared. The rightmost figures exhibit negligible variation of K with varying r.

Reference

(1) Andrei, E. Y.; MacDonald, A. H. Graphene bilayers with a twist. Nat. Mater. 2020, 19 (12), 1265-1275. DOI: 10.1038/s41563-020-00840-0.

(2) Mesple, F.; Walet, N. R.; Trambly de Laissardiere, G.; Guinea, F.; Dosenovic, D.; Okuno, H.; Paillet, C.; Michon, A.; Chapelier, C.; Renard, V. T. Giant Atomic Swirl in Graphene Bilayers with Biaxial Heterostrain. Adv. Mater. 2023, 35 (41), 2306312. DOI: 10.1002/adma.202306312.

(3) Bagchi, S.; Johnson, H. T.; Chew, H. B. Rotational stability of twisted bilayer graphene. Phys. Rev. B 2020, 101 (5), 054109. DOI: 10.1103/PhysRevB.101.054109.

(4) Huang, S.; Liang, L.; Ling, X.; Puretzky, A. A.; Geohegan, D. B.; Sumpter, B. G.; Kong, J.; Meunier, V.; Dresselhaus, M. S. Low-Frequency Interlayer Raman Modes to Probe Interface of Twisted Bilayer MoS2. Nano Lett. 2016, 16 (2), 1435-1444. DOI: 10.1021/acs.nanolett.5b05015.

(5) Jung, J.; Laksono, E.; DaSilva, A. M.; MacDonald, A. H.; Mucha-Kruczyński, M.; Adam, S. Moiré band model and band gaps of graphene on hexagonal boron nitride. Phys. Rev. B 2017, 96 (8), 085442. DOI: 10.1103/PhysRevB.96.085442.

(6) van Wijk, M. M.; Schuring, A.; Katsnelson, M. I.; Fasolino, A. Moiré Patterns as a Probe of Interplanar Interactions for Graphene on h-BN. Phys. Rev. Lett. 2014, 113 (13), 135504. DOI: 10.1103/PhysRevLett.113.135504.

(7) Leven, I.; Maaravi, T.; Azuri, I.; Kronik, L.; Hod, O. Interlayer Potential for Graphene/h-BN Heterostructures. J. Chem. Theory Comput. 2016, 12 (6), 2896-2905. DOI: 10.1021/acs.jctc.6b00147.

(8) Kolmogorov, A. N.; Crespi, V. H. Registry-dependent interlayer potential for graphitic systems. Phys. Rev. B 2005, 71 (23), 235415. DOI: 10.1103/PhysRevB.71.235415.

(9) Brenner, D. W.; Shenderova, O. A.; Harrison, J. A.; Stuart, S. J.; Ni, B.; Sinnott, S. B. A second-generation reactive empirical bond order (REBO) potential energy expression for hydrocarbons. J. Phys.: Condens. Matter 2002, 14, 783-802. DOI: 10.1088/0953-8984/14/4/312.

(10) Ouyang, W.; Mandelli, D.; Urbakh, M.; Hod, O. Nanoserpents: Graphene Nanoribbon Motion on Two-Dimensional Hexagonal Materials. Nano Lett. 2018, 18 (9), 6009-6016. DOI: 10.1021/acs.nanolett.8b02848.

(11) Tersoff, J. New empirical approach for the structure and energy of covalent systems. Phys. Rev. B 1988, 37 (12), 6991-7000. DOI: 10.1103/PhysRevB.37.6991.

(12) Ostadhossein, A.; Rahnamoun, A.; Wang, Y.; Zhao, P.; Zhang, S.; Crespi, V. H.; van Duin, A. C. T. ReaxFF Reactive Force-Field Study of Molybdenum Disulfide (MoS2). J. Phys. Chem. Lett. 2017, 8 (3), 631-640. DOI: 10.1021/acs.jpclett.6b02902.

(13) Ribeiro-Palau, R.; Zhang, C.; Watanabe, K.; Taniguchi, T.; Hone, J.; Dean, C. R. Twistable electronics with dynamically rotatable heterostructures. Science 2018, 361 (6403), 690-693. DOI: 10.1126/science.aat6981.

(14) Dai, Z.; Liu, L.; Zhang, Z. Strain Engineering of 2D Materials: Issues and Opportunities at the Interface. Adv. Mater. 2019, 31 (45), 1805417. DOI: 10.1002/adma.201805417.

(15) Wang, J.; Namburu, R.; Dubey, M.; Dongare, A. M. Origins of Moiré Patterns in CVD-grown MoS2 Bilayer Structures at the Atomic Scales. Sci. Rep. 2018, 8 (1), 9439. DOI: 10.1038/s41598-018-27582-z.

(16) Wang, K.; Qu, C.; Wang, J.; Ouyang, W.; Ma, M.; Zheng, Q. Strain Engineering Modulates Graphene Interlayer Friction by Moiré Pattern Evolution. ACS Appl. Mater. Interfaces 2019, 11 (39), 36169-36176. DOI: 10.1021/acsami.9b09259.
(17) Nam, N. N. T.; Koshino, M. Lattice relaxation and energy band modulation in twisted bilayer graphene. Phys. Rev. B 2017, 96 (7), 075311. DOI: 10.1103/PhysRevB.96.075311.
(18) Zhang, K.; Tadmor, E. B. Structural and electron diffraction scaling of twisted graphene bilayers. J. Mech. Phys. Solids 2018, 112, 225-238. DOI: 10.1016/j.jmps.2017.12.005.
(19) Carr, S.; Massatt, D.; Torrisi, S. B.; Cazeaux, P.; Luskin, M.; Kaxiras, E. Relaxation and domain formation in incommensurate two-dimensional heterostructures. Phys. Rev. B 2018, 98 (22), 224102. DOI: 10.1103/PhysRevB.98.224102.
(20) Zhu, S.; Pochet, P.; Johnson, H. T. Controlling Rotation of Two-Dimensional Material Flakes. ACS Nano 2019, 13 (6), 6925-6931. DOI: 10.1021/acsnano.9b01794.